FRONTIERS OF PHYSICS

RESEARCH ARTICLE
Volume 19 / Issue 3 / 33210 / 2024

Magnetic and electrical transport study of the intrinsic magnetic topological insulator $MnBi_2Te_4$ with Ge doping

Qingwang Bai, Mingxiang Xu†

School of Physics, Southeast University, Nanjing 211189, China
Corresponding author. E-mail: †mxxu@seu.edu.cn
Received November 14, 2023; accepted April 8, 2024

ABSTRACT

As an intrinsic magnetic topological insulator with magnetic order and non-trivial topological structure, $MnBi_2Te_4$ is an ideal material for studying exotic topological states such as quantum anomalous Hall effect and topological axion insulating states. Here, we carry out magnetic and electrical transport measurements on $(Mn_{1-x}Ge_x)Bi_2Te_4$ (x = 0, 0.15, 0.30, 0.45, 0.60, and 0.75) single crystals. It is found that with increasing x, the dilution of magnetic moments gradually weakens the antiferromagnetic exchange interaction. Moreover, Ge doping reduces the critical field of ferromagnetic ordering, which may provide a possible way to implement the quantum anomalous Hall effect at lower magnetic field. Electrical transport measurements suggest that electrons are the dominant charge carriers, and the carrier density increases with the Ge doping ratio. Additionally, the Kondo effect is observed in the samples with x = 0.45, 0.60, and 0.75. Our results suggest that doping germanium is a viable way to tune the magnetic and electrical transport properties of $MnBi_2Te_4$, opening up the possibility of future applications in magnetic topological insulators.

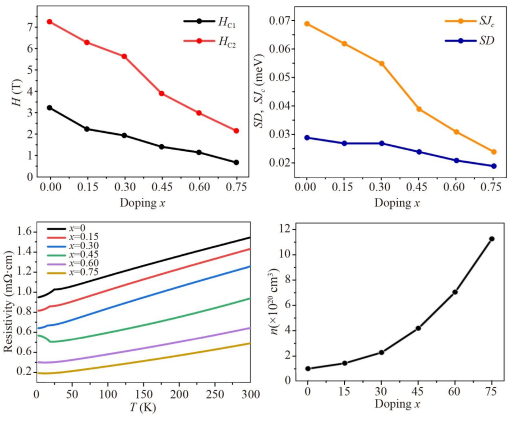

Keywords $MnBi_2Te_4$, intrinsic magnetic topological insulator, transition points, Kondo effect

1 Introduction

Quantum anomalous Hall effect (QAHE) is a representative topological quantum phenomenon, demonstrating quantized Hall resistance and near-zero longitudinal resistance in the absence of an external magnetic field, suggesting broad application prospects in dissipationless electronic devices [1–3]. Among the various approaches proposed to achieve the QAHE, the magnetic topological insulator emerges as the most favorable system based on both experimental and theoretical investigations, primarily owing to its intrinsically robust spin–orbit coupling [4, 5]. QAHE was first realized in thin films of $(Bi, Sb)_2Te_3$ doped with Cr in 2013 [6]. However, the observed QAHE is limited to temperatures as low as several tens of millikelvin due to the presence of inhomogeneity or disorder caused by random magnetic doping. Therefore, there is a strong motivation to find intrinsic magnetic topological insulators (TIs) that can exhibit high-temperature QAHE. In this regard, $MnBi_2Te_4$, a recently discovered intrinsic antiferromagnetic (AFM) TI, has attracted considerable attention [7–9].

$MnBi_2Te_4$ has a van der Waals (vdW) layered structure, which consists of Te–Bi–Te–Mn–Te–Bi–Te septuple layers (SLs) stacking along the c-axis [10]. Magnetic measurements reveal that the Mn ions exhibit a high-spin $S = 5/2$ configuration with a magnetic moment of approximately $5\mu_B$, and an antiferromagnetic transition at 24 K is observed. Consequently, $MnBi_2Te_4$ presents a unique natural heterostructure comprising antiferromag-

Higher Education Press

https://doi.org/10.1007/s11467-024-1408-5

netic planes intertwined with layers of TIs [11–16]. Furthermore, theoretical calculations suggest that the $MnBi_2Te_4$ may exhibit QAHE states, with a gap of approximately 50–80 meV, significantly exceeding that of a magnetically doped topological insulator, indicating the potential for achieving QAHE at higher temperatures [17–19]. However, achieving a ferromagnetic (FM) state in $MnBi_2Te_4$ necessitates an ultra-high magnetic field, making it challenging to realize a QAHE state under low magnetic fields [20]. One effective approach is to substitute the Mn element with nonmagnetic ions (such as Pb) to reduce the critical field required to align the magnetic moments to the ferromagnetic state [21, 22]. However, studies on the nonmagnetic ionic substitution of Mn in $MnBi_2Te_4$ are still few and lack comprehensive analysis, hence further studies are needed.

In this study, we conducted a comprehensive analysis to investigate the impact of Ge doping on the magnetic and electrical transport properties of the antiferromagnetic topological insulator $MnBi_2Te_4$. To achieve this, we prepared single crystals of $(Mn_{1-x}Ge_x)Bi_2Te_4$ with different Ge doping concentrations (x = 0, 0.15, 0.30, 0.45, 0.60, and 0.75). It was observed that Ge doping significantly influenced the antiferromagnetic ordering, as evidenced by the decrease in the Néel temperature (T_N) with increasing Ge concentration. This suggests that magnetic engineering is feasible in $(Mn_{1-x}Ge_x)Bi_2Te_4$. Furthermore, the transition points were found to decrease compared to pure $MnBi_2Te_4$. Since a Chern insulator can be observed at the ferromagnetic regime, reducing the transition field in $MnBi_2Te_4$ can realize a QAHE state at a relatively low magnetic field, beneficial to its further applications in devices and spintronics [23–25]. Additionally, Hall resistivity measurements show an increase in the n-type carrier density as the increase of doping concentration, indicating the modulation of carrier density via Ge doping.

2 Experimental details

Single crystals of $(Mn_{1-x}Ge_x)Bi_2Te_4$ of high quality were grown by the self-flux method. Mixtures of $(Mn_{1-x}+Ge_x)Te$ and Bi_2Te_3 powder (nominal x = 0, 0.15, 0.30, 0.45, 0.60, and 0.75) with the 1:1 ratio were placed in an alumina crucible, which was then sealed in an evacuated quartz tube. Subsequently, the mixture was heated to 900 °C over 15 hours and maintained at that temperature for 12 hours. Finally, it was slowly cooled to 591 °C at a rate of 1 °C per hour. and annealed for at least 14 days. The crystal structure of all samples was characterized by X-ray diffraction (XRD) on a commercial Rigaku diffractometer with Cu Kα radiation (λ = 1.5403 Å). A field emission scanning electron microscope (FEI Inspect F50) equipped with an energy dispersive X-ray spectroscopy (EDS, INCA spectrometer) detector was used to visualize the morphology of the surfaces and the distribution of the elements in the composites. Transport and magnetic properties were determined using a physical property measurement system (PPMS-9, Quantum Design).

3 Results and discussion

Ge-doped $MnBi_2Te_4$ crystals exhibit a layered rhombohedral crystal structure with the space group R-3m [26, 27], composed of stacking SLs Te–Bi–Te–X–Te–Bi–Te (X = Mn/Ge) as displayed in Fig. 1(a). Figure 1(b) shows the XRD data of $(Mn_{1-x}Ge_x)Bi_2Te_4$ single crystals. It can be observed that all samples display explicit reflections from the (0 0 l) plane and without any impurity peaks, confirming phase purity for all the crystals. The as-grown samples exhibit a smooth and shiny surface as displayed in the inset (left) of Fig. 1(b). The inset (right) of Fig. 1(b) displays the enlarging pattern of (0 0 2 1) diffraction peaks, which shift left with the Ge contents increase. The results show that Ge-doped $MnBi_2Te_4$ crystals have lattice expansion, which can be attributed to the larger radius of the Ge ion (0.73 Å) compared to that of the Mn ion (0.67 Å) by 9%. The Bi-normalized EDS images of $(Mn_{1-x}Ge_x)Bi_2Te_4$ with different amounts of germanium substitution are shown in Fig. 1(c), which shows that the stoichiometric ratio of Mn:Ge:Bi:Te is close to the nominal ratio. These results suggest that Ge successfully substitutes Mn in $MnBi_2Te_4$. The scanning electron microscope (SEM) image of the surface of the $(Mn_{0.85}Ge_{0.15})Bi_2Te_4$ sample is shown in Fig. 1(d). The crystal exhibits a smooth surface with a visible layered structure, consistent with findings reported in previous studies [10–15]. Figure 1(e) shows the corresponding EDS mapping, which reveals that Mn, Ge, Bi, and Te elements are homogeneously distributed in the crystal. Figure 1(f) demonstrates the high-resolution TEM image of the $(Mn_{0.85}Ge_{0.15})Bi_2Te_4$ sample. The atomic fringes from the (110) lattice plane with a spacing of 0.215 nm are clearly shown, and the atomic fringes are relatively intact without significant deformation and dislocation. This indicates that the studied samples are high quality single crystals.

To investigate the impact of Ge doping on the magnetic properties of $MnBi_2Te_4$, we conducted comprehensive magnetic measurements on different Ge doping ratios. In Fig. 2(a), the zero-field-cooled (ZFC) and field-cooled (FC) magnetic susceptibility (χ) is plotted against temperature for the $(Mn_{1-x}Ge_x)Bi_2Te_4$ samples under out-of-plane ($H//c$) and in-plane ($H//ab$) magnetic fields. The ZFC and FC plots overlap for all materials, indicating negligible magnetic hysteresis. As displayed in the figure, the magnetic susceptibility of $MnBi_2Te_4$ (x = 0) rises as temperature decreases under a magnetic field of 1 T, peaking at a Néel temperature (T_N) of 24.7 K before

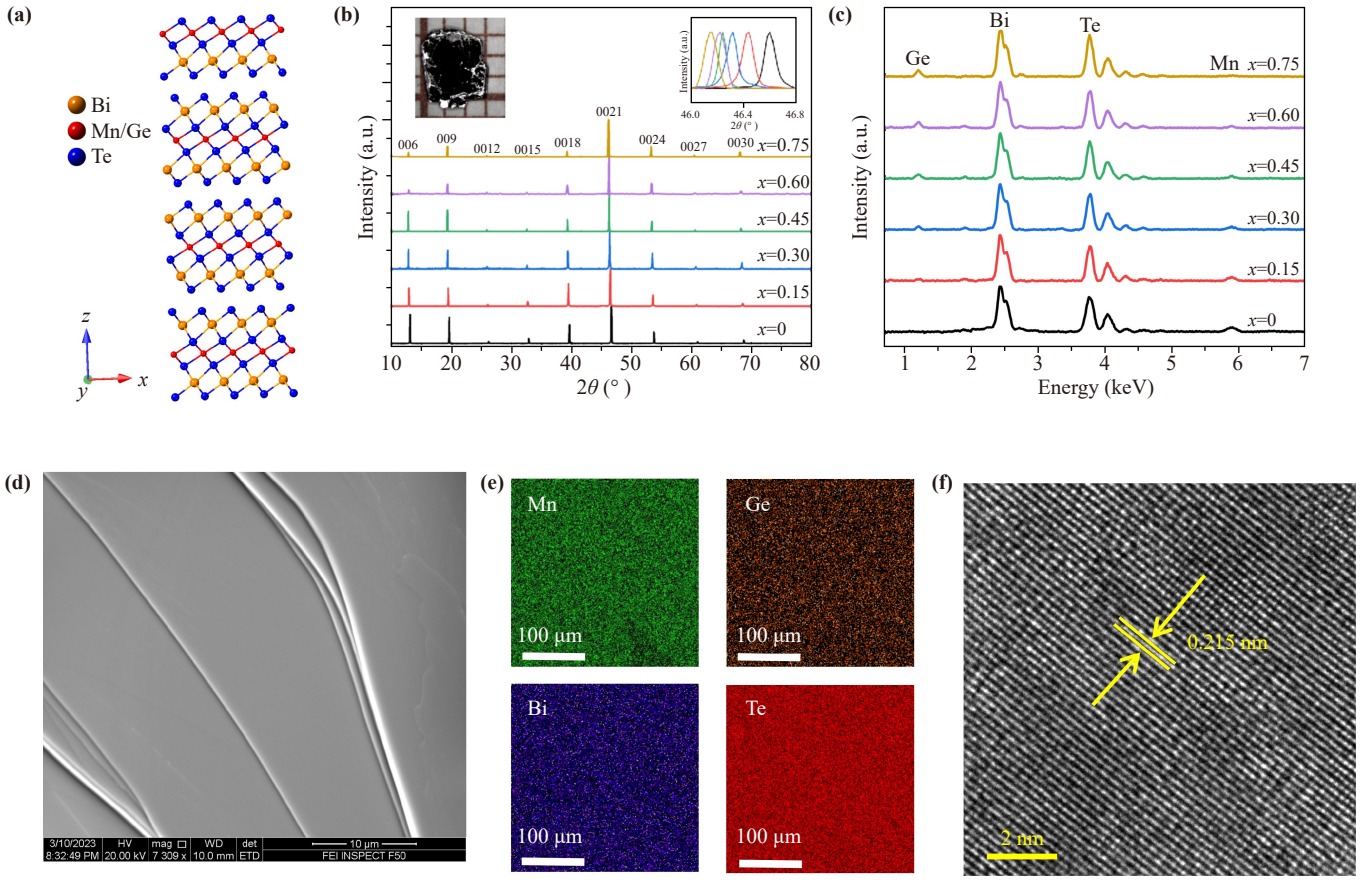

Fig. 1 **(a)** Crystal structure of $(Mn_{1-x}Ge_x)Bi_2Te_4$. **(b)** Single crystal X-ray diffraction pattern for samples with different germanium substitutions. The top left inset: The photograph of the crystal on a millimeter grid. The top right inset: A magnified view of (0 0 2 1) diffraction peaks. **(c)** EDS curves of the crystals with different nominal Ge doping levels x. **(d)** SEM image of a $(Mn_{0.85}Ge_{0.15})Bi_2Te_4$ crystal surface. **(e)** EDS element mapping of the $(Mn_{0.85}Ge_{0.15})Bi_2Te_4$ crystal. **(f)** The high-resolution TEM image of the $(Mn_{0.85}Ge_{0.15})Bi_2Te_4$ crystal.

sharply declining, which is in good consistency with previous reports [28, 29]. For $H//c$, the magnetic susceptibility curves of samples with different ratios of Ge can clearly show peak characteristics, indicating the AFM magnetic transition with T_N in these samples. After T_N, the magnetic susceptibility decreases significantly in the $H//c$ direction, whereas it only shows a slight decline in the $H//ab$ direction. This notable variance in χ between the out-of-plane and in-plane orientations indicates an anisotropy in the antiferromagnetic order. Additionally, the AFM magnetic transition weakens and ultimately vanishes with increasing applied magnetic field, attributed to the suppression of inter-layer AFM coupling induced by an external magnetic field [9]. Furthermore, with increasing Ge substitution in $(Mn_{1-x}Ge_x)Bi_2Te_4$, the 2D ferromagnetic sublattice becomes diluted, resulting in a gradual decrease in T_N as shown in Fig. 2(d). The reduction of Néel temperature indicates an obvious weakening of inter-layer AFM coupling.

Figures 2(b) and (c) show the temperature dependence of the inverse magnetic susceptibility (χ^{-1}) with $H//c$ and $H//ab$ when $H = 1$ T. The χ^{-1} of all samples above Néel temperature exhibits a linear relationship with temperature, conforming to the Curie–Weiss law expressed as $\chi = C/(T - \theta_W)$, where C is the Curie constant and θ_W is the Curie–Weiss temperature. By linearly fitting χ^{-1} versus T, we obtained the effective magnetic moment $\mu_{eff} = 5.5\mu_B$/Mn for $MnBi_2Te_4$, which is consistent with the theoretical value of $5.9\mu_B$ for high-spin Mn^{2+} ions with $3d^5$ configuration [30]. The θ_W for each composition as a function of Ge concentration is plotted in Fig. 2(e). Distinct θ_W temperatures were observed for the out-of-plane and in-plane field directions in samples with $x = 0$, 0.15, and 0.30 Ge concentrations, while at higher Ge concentrations, both θ_W approached equality, attributed to the reduction of magnetic anisotropy with increasing Ge concentration. Furthermore, the strength of ferromagnetic exchange interaction concerning antiferromagnetic can be confirmed from the ratio of θ_W/T_N, which equals $(J_F + J_{AF})/(J_F - J_{AF})$ [31]. Here J_F represents the ferromagnetic exchange coupling and J_{AF} represents the antiferromagnetic exchange coupling. The calculated J_{AF}/J_F ratio as a function of doping concentration is

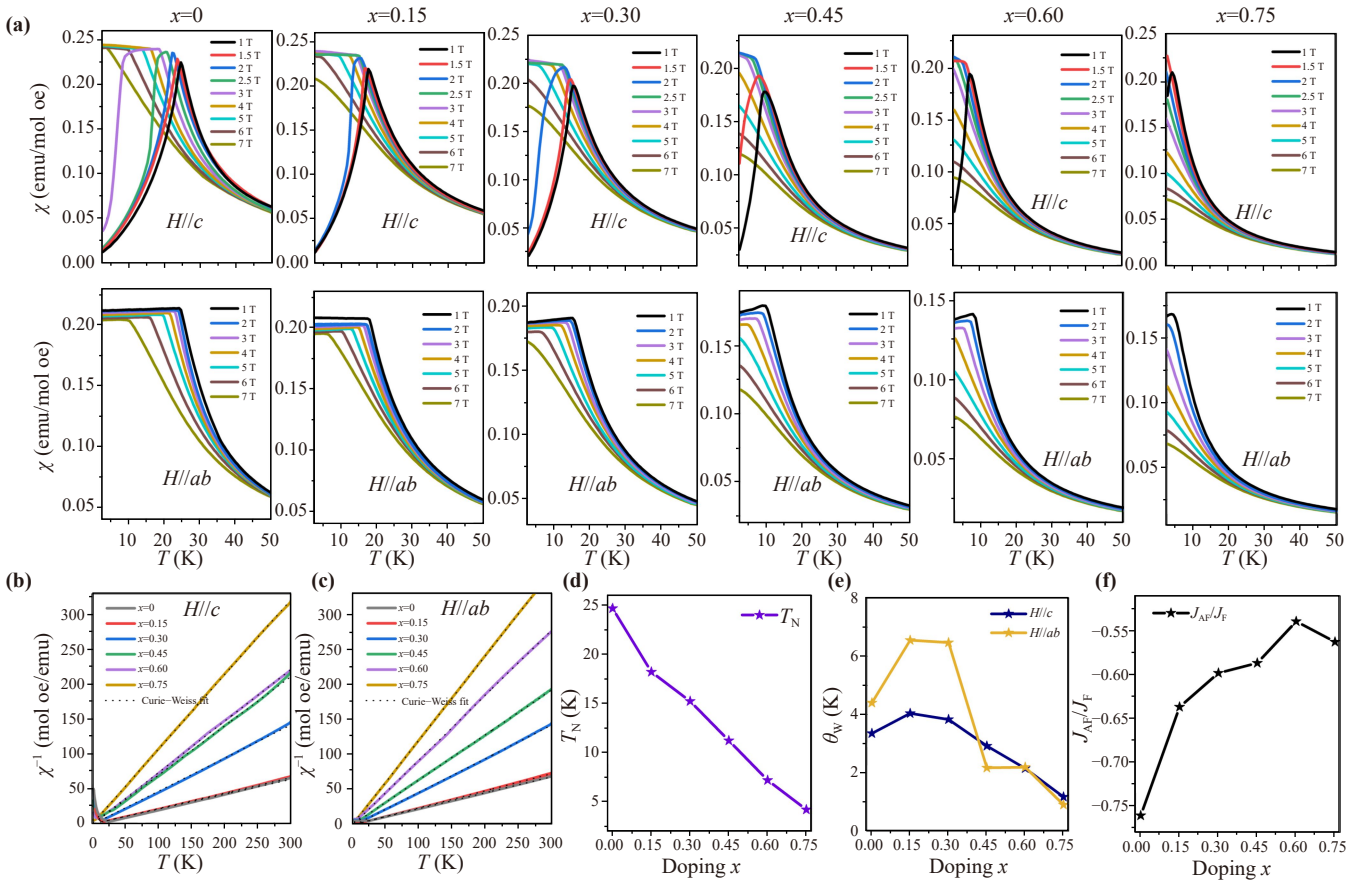

Fig. 2 **(a)** Field-cooled and zero field-cooled curves of $(Mn_{1-x}Ge_x)Bi_2Te_4$ in various magnetic fields with $H//c$ and $H//ab$. **(b, c)** Temperature dependence of inverse susceptibility for samples with $H//c$ and $H//ab$, respectively. Doping dependent **(d)** Néel temperature (T_N), **(e)** Curie temperature (θ_W) for $H//c$ and $H//ab$ and **(f)** J_{AF}/J_F for $H//c$.

plotted in Fig. 2(f). It is obvious that with the increase of Ge concentration, the absolute value of the J_{AF}/J_F ratio gradually decreased, indicating a weakening of the AFM coupling in the sample. This finding is consistent with the reasons for the decrease in T_N mentioned above.

The isothermal magnetization versus magnetic field (M–H) curves under $H//c$ and $H//ab$ are displayed in Figs. 3(a)–(f). The M–H curve obtained for the $H//ab$ orientation reveals lower magnetization values with a linear field dependence, implying that the c axis serves as the easy axis for magnetization. For $H//c$, as the field increases, all samples below T_N exhibit the evolution of the spin-structure from AFM state to canted AFM state (H_{c1}), and finally to a polarized FM state (H_{c2}). The two spin-flop transition points are marked with red and black triangles in Figs. 3(a)–(f), and the positions of the transition points corresponding to each sample are extracted in Fig. 3(g). It illustrates that the spin-flop transition points decrease as the Ge doping level increases, indicating a significant weakening of the antiferromagnetic exchange coupling, which corresponds with the reduction of T_N. Pb and Sn doping can also achieve the effect of reducing the spin-flop transition point of $MnBi_2Te_4$, suggesting that using non-magnetic ions instead of manganese is an effective strategy to reduce the spin-flop transition point [21, 22]. In conclusion, substituting Ge for Mn in $MnBi_2Te_4$ crystals will lower the critical field of ferromagnetic ordering, which will help realize QAHE states under the low field, favoring its practical application to dissipationless electronic devices and spintronics [15–18].

For a uniaxial antiferromagnet, the saturation field under $H//c$ and $H//ab$ can be expressed in terms of the interlayer antiferromagnetic exchange (J_c) and single-ion anisotropy (D) as $g\mu_B H_c = 2zSJ_c - 2SD$ and $g\mu_B H_{ab} = 2zJ_c + 2SD$, respectively, where $g = 2$, $S = 5/2$, and $z = 6$ is the coordination number for Mn to other Mn in layers above and below. Therefore, J_c and D can be calculated as $SJ_c = (4z)^{-1} g\mu_B J_c(H_c + H_{ab})$ and $SD = \frac{1}{4} g\mu_B(H_{ab} - H_c)$, respectively. The calculated SJ_c and SD are shown in Fig. 3(h). It is obvious that both SJ_c and SD decrease with increasing Ge content, which was consistent with the situation of Sb doping [32]. The decrease of SJ_c further confirms that Ge doping reduces the interlayer antiferromagnetic coupling of the sample.

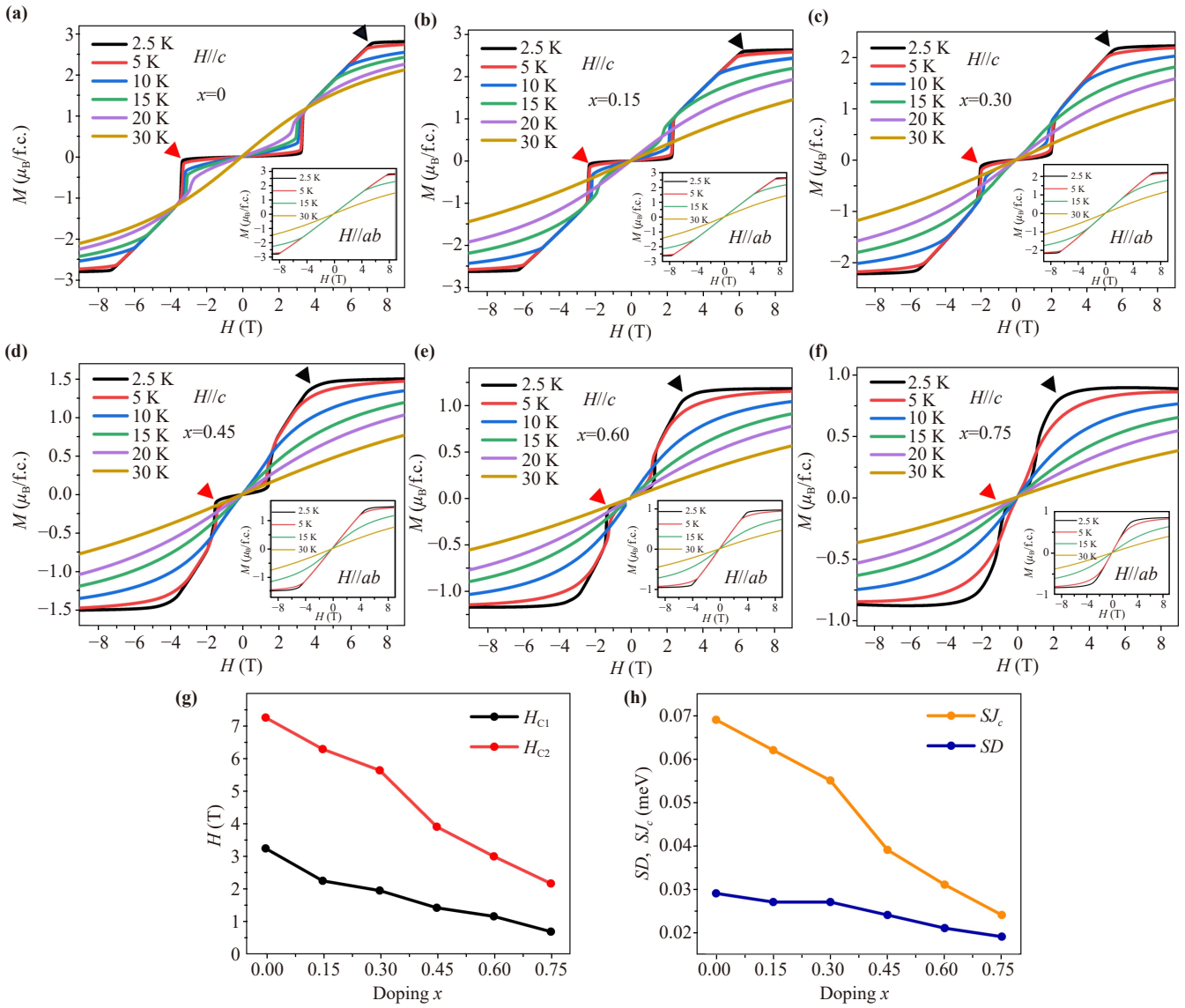

Fig. 3 **(a–f)** Magnetization vs. magnetic field (M–H) curves of the different Ge doped ratio samples with $H//c$ and $H//ab$ (inset). Red triangles: Transition points of the antiferromagnetic to canted antiferromagnetic (H_{c1}). Black triangles: Canted antiferromagnetic to ferromagnetic (H_{c2}). **(g)** Corresponding H_{c1} and H_{c2} of samples with different x derived from the magnetism measurements in (a–f). **(h)** Compositional interlayer magnetic interaction (SJ_c) and single-ion anisotropy (SD) with different x.

In addition, the reduction of SD is consistent with the conclusion above that Ge doping reduces the magnetic anisotropy of the sample.

To further study the transport properties of the Ge-doped $MnBi_2Te_4$ samples, we measured the temperature dependence of resistivity over a range of 2.5 to 300 K, as depicted in Fig. 4(a). The resistivity peak temperature of the sample for $x = 0$, 0.15, and 0.30 is consistent with T_N observed in the magnetic property measurement. This peak is caused by spin scattering due to strong spin fluctuations at temperatures approaching T_N. It is noteworthy that at $x = 0.45$, 0.60, and 0.75, this peak is absent in the sample and we observe an anomalous upturn in the resistivity at low temperatures. In principle, three primary reasons account for the resistance upturn: electron–electron interaction (EEI), weak localization (WL), and Kondo effect [33–36]. Among the mechanisms mentioned, the resistivity correction from EEI encompasses both singlet and triplet terms. In theory, the singlet term remains independent of the field, while the triplet term exhibits field dependency unless spin-relaxation processes are disregarded. Therefore, when strong spin scattering is present or the triplet term is significantly smaller than the singlet term, the EEI becomes insensitive to the magnetic field. Even if the triplet term contributes notably to the overall EEI

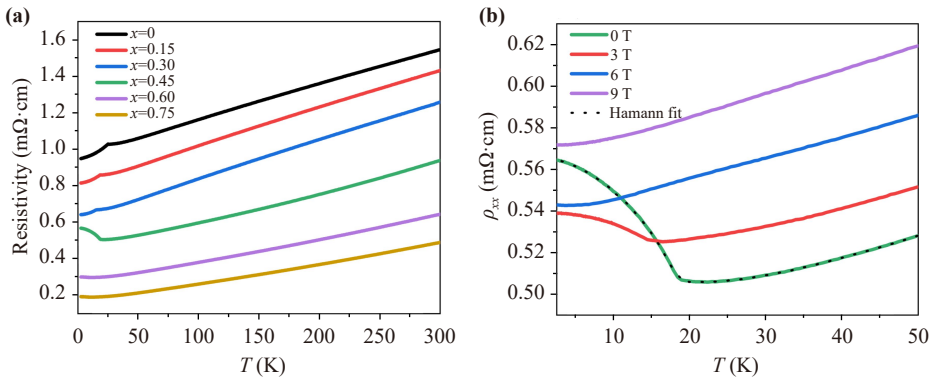

Fig. 4 **(a)** Temperature-dependent resistivity of $(Mn_{1-x}Ge_x)Bi_2Te_4$ with $x = 0$, 0.15, 0.30, 0.45, 0.60 and 0.75. **(b)** Temperature-dependent resistivity for $(Mn_{0.55}Ge_{0.45})Bi_2Te_4$ under different magnetic fields. The dashed line represents the Hamann fit.

correction, the magnitude of the resistance upturn can be influenced by the magnetic field but not completely suppressed. As a result, it is possible to distinguish the electron–electron interaction by comparing the temperature dependence of resistivity under varying applied magnetic fields [37, 38]. Figure 4(b) presents the temperature-dependent resistivity of $(Mn_{0.55}Ge_{0.45})Bi_2Te_4$ under different magnetic fields. The upturn behaviors gradually diminish with the increment of the magnetic field and vanish when the field exceeds 6 T. This observation rules out the dominance of EEI in the low-temperature transport characteristics of the sample. Traditionally, WL phenomena are observed in low-dimensional systems like thin films and nanowires owing to the higher probability of scattering rates leading to quantum interference [39]. Moreover, the conductivity (σ) does not adhere well to the weak localization formulation $\sigma = \sigma_0 + kT^{p/2}$ where $k = 2e^2/(ah\pi^2)$ and the factor a is defined in terms of Thoules inelastic collision length (L_{Th}) as $L_{\mathrm{Th}} = aT^{-p/2}$ for $p = 2$, 3, and 3/2 [39]. Thus, the discussion can also exclude the WL effect. Finally, we conclude that the upturns of the resistance are dominated by the Kondo effect.

For systems exhibiting the Kondo effect, the resistive upturn at low temperatures can be modeled using Hamann's equation [40, 41]:

$$\rho(T) = \rho_0 + qT^2 + pT^5 + \rho_{\mathrm{K}}\{1 - \ln(T/T_{\mathrm{K}}) \cdot [\ln^2(T/T_{\mathrm{K}}) + S(S+1)\pi^2]^{-1/2}\},$$

where both p and q are fitting parameters; ρ_{K}, T_{K}, and S represent the temperature-independent resistivity, the Kondo temperature, and the spin of magnetic impurities, respectively. As illustrated in Fig. 4(b), the Hamann fitting provides a satisfactory description of the experimental data, resulting in $T_{\mathrm{K}} = 18.63$ K and $S = 0.13$. Thus, we emphasize that the upturns of the resistance are dominated by the Kondo effect.

Figures 5(a)–(f) display the magneto-resistivity (MR) curves obtained at various temperatures. From Fig. 5(a), at $x = 0$, there is a noticeable decrease in ρ_{xx} over the critical magnetic field of 3.2 T below T_{N}, and another change in slope occurs at a critical field of 7.3 T. These critical fields, as determined from the MR data, align closely with the values of H_{c1} and H_{c2} obtained from the magnetic measurement. Above the Néel temperature, noticeable negative magnetoresistivity is observed in samples with $x = 0$, 0.15, and 0.30 [as shown in Figs. 5(a)–(c)], owing to the strong antiferromagnetic spin fluctuation. For samples with $x = 0.45$, 0.60, and 0.75, the parabolic field above Néel temperature is dependent on MR due to its paramagnetism.

To study the impact of Ge doping on the carrier density in the system, the Hall resistivity ρ_{yx} was measured for samples with varying doping ratios, as depicted in Figs. 6(a)–(f). All the Hall resistivity curves have a negative slope indicating that electrons are the dominant charge carriers. The carrier density can be calculated by the equation $n = 1/(eR_{\mathrm{H}})$, where n represents the carrier density and R_{H} represents the Hall coefficient. Figure 6(g) displays the carrier density of each sample at 2.5 K. It is clear that the n-type carrier density increases with the doping concentration, indicating that the carrier density of the sample is successfully modulated by Ge doping. The carrier density increase can also be identified from the plots of temperature-dependent resistivity for materials. As shown in Fig. 4(a), at the same temperature, the resistivity of the sample gradually decreases with the increase of the Ge doping ratio.

Ge doping can affect not only the magnetic and transport properties but also the topological properties of $MnBi_2Te_4$. In the study conducted by Estyunina *et al.* [42], they used *ab-initio* calculations to determine that when the Ge concentration exceeds 50%, there is an absence of bulk band inversion at the Γ-point for the contributions of Te p_z and Bi p_z, along with significant spatial redistribution of states at the edges of the band gap into the bulk [42]. This observation suggests a topological phase transition in the system.

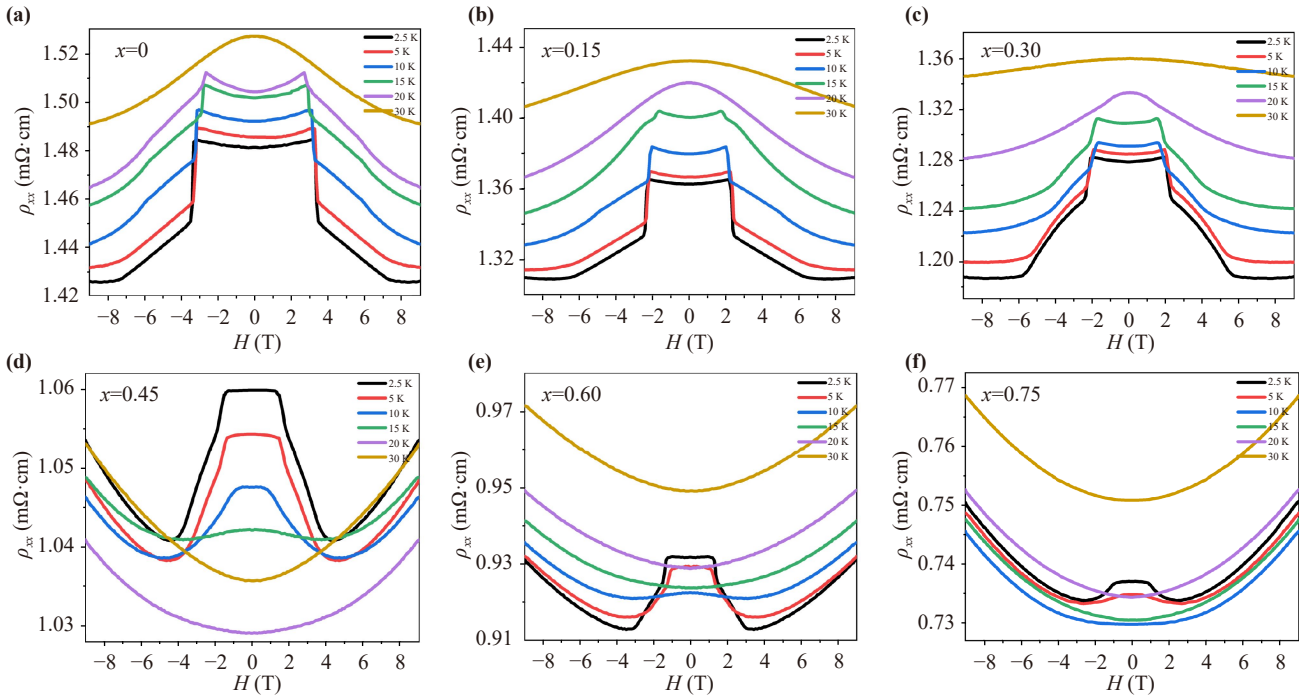

Fig. 5 Magnetic resistance versus magnetic field for various temperatures of the sample: **(a)** $x = 0$; **(b)** $x = 0.15$; **(c)** $x = 0.30$; **(d)** $x = 0.45$; **(e)** $x = 0.60$; **(f)** $x = 0.75$.

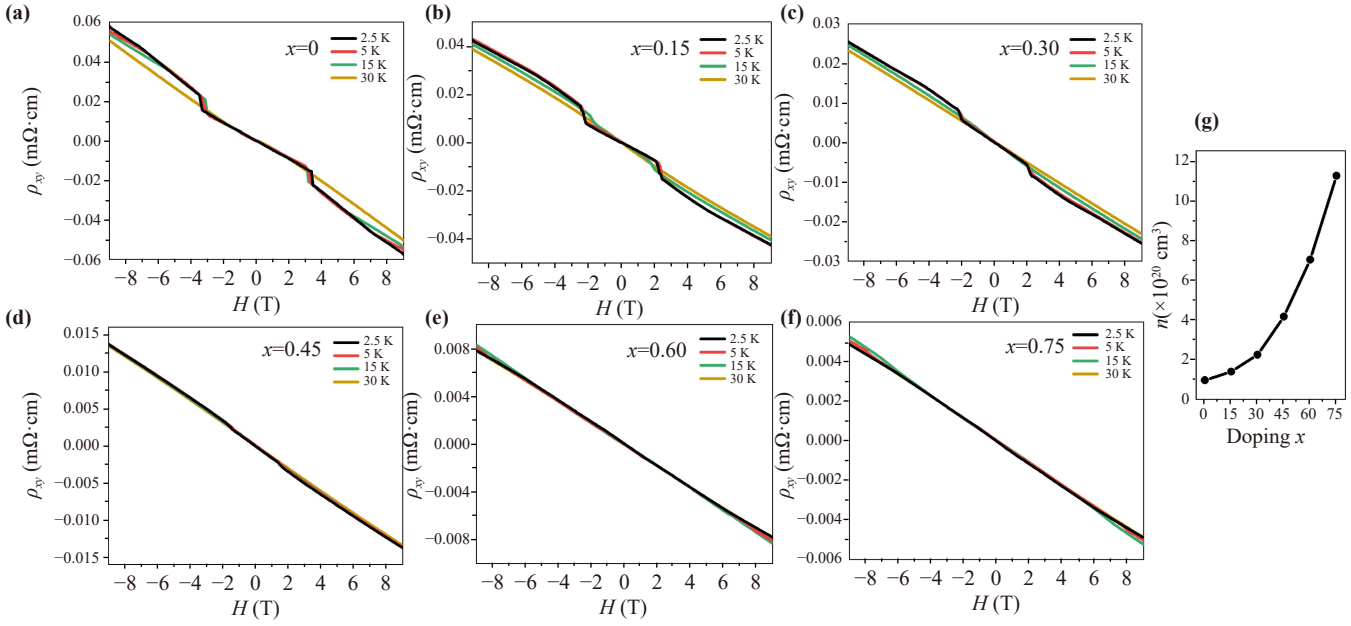

Fig. 6 **(a–f)** Magnetic field dependence of the Hall resistivity from $x = 0$ to 0.75. **(g)** Carrier densities extracted from the Hall resistivity.

4 Conclusions

In conclusion, we have synthesized a series of high-quality single crystals of Ge-doped $MnBi_2Te_4$. We find that Ge substitutes for Mn in $MnBi_2Te_4$, which can effectively weaken robust AFM coupling, thereby reducing the external magnetic field that aligns the magnetic moments into the ferromagnetic state, which may provide a possible way to implement the QAHE at lower magnetic field. Electrical transport measurements suggest that the mainly transport dominated carriers are n-type, and the density of the carrier increases with the

doping concentration. Additionally, the Kondo effect is observed in the samples with $x = 0.45$, 0.60, and 0.75. Our studies on Ge-doped $MnBi_2Te_4$ reveal that element doping effectively modulates the magnetic and transport properties of magnetic topological insulators. This research provides insights into optimizing and achieving the QAHE and other related quantum topological effects.

Declarations The authors declare that they have no competing interests and there are no conflicts.

Acknowledgements This work was supported by the National Key R&D Program of China (Grant No. 2018YFA0704300) and the Natural Science Foundation of Jiangsu Province of China (Grant No. BK20201285).

References

1. R. Li, J. Wang, X. L. Qi, and S. C. Zhang, Dynamical axion field in topological magnetic insulators, *Nat. Phys.* 6, 284 (2010)
2. Y. Wang, F. Zhang, M. Zeng, H. Sun, Z. Hao, Y. Cai, H. Rong, C. Zhang, C. Liu, X. Ma, L. Wang, S. Guo, J. Lin, Q. Liu, C. Liu, and C. Chen, Intrinsic magnetic topological materials, *Front. Phys.* 18(2), 21304 (2023)
3. X. Zhu, Y. Chen, Z. Liu, Y. Han, and Z. Qiao, Valley-polarized quantum anomalous Hall effect in van der Waals heterostructures based on monolayer jacutingaite family materials, *Front. Phys.* 18(2), 23302 (2023)
4. W. Zhao, D. Cortie, L. Chen, Z. Li, Z. Yue, and X. Wang, Quantum oscillations in iron-doped single crystals of the topological insulator Sb_2Te_3, *Phys. Rev. B* 99(16), 165133 (2019)
5. Y. Xu, I. Miotkowski, C. Liu, J. Tian, H. Nam, N. Alidoust, J. Hu, C. K. Shih, M. Z. Hasan, and Y. P. Chen, Observation of topological surface state quantum Hall effect in an intrinsic three-dimensional topological insulator, *Nat. Phys.* 10(12), 956 (2014)
6. C. Z. Chang, J. Zhang, X. Feng, J. Shen, Z. Zhang, M. Guo, K. Li, Y. Ou, P. Wei, L. L. Wang, Z. Q. Ji, Y. Feng, S. Ji, X. Chen, J. Jia, X. Dai, Z. Fang, S. C. Zhang, K. He, Y. Wang, L. Lu, X. C. Ma, and Q. K. Xue, Experimental observation of the quantum anomalous Hall effect in a magnetic topological insulator, *Science* 340, 167 (2013)
7. D. Zhang, M. Shi, T. Zhu, D. Xing, H. Zhang, and J. Wang, Topological axion states in the magnetic insulator $MnBi_2Te_4$ with the quantized magnetoelectric effect, *Phys. Rev. Lett.* 122(20), 206401 (2019)
8. M. M. Otrokov, I. P. Rusinov, M. Blanco-Rey, M. Hoffmann, A. Yu. Vyazovskaya, S. V. Eremeev, A. Ernst, P. M. Echenique, A. Arnau, and E. V. Chulkov, Unique thickness-dependent properties of the van der Waals interlayer antiferromagnet $MnBi_2Te_4$ films, *Phys. Rev. Lett.* 122(10), 107202 (2019)
9. J. Q. Yan, Y. H. Liu, D. S. Parker, Y. Wu, A. A. Aczel, M. Matsuda, M. A. McGuire, and B. C. Sales, A-type antiferromagnetic order in $MnBi_4Te_7$ and $MnBi_6Te_{10}$ single crystals, *Phys. Rev. Mater.* 4(5), 054202 (2020)
10. K. Y. Chen, B. S. Wang, J. Q. Yan, D. S. Parker, J. S. Zhou, Y. Uwatoko, and J. G. Cheng, Suppression of the antiferromagnetic metallic state in the pressurized $MnBi_2Te_4$ single crystal, *Phys. Rev. Mater.* 3(9), 094201 (2019)
11. C. Y. Pei, Y. Y. Xia, J. Z. Wu, Y. Zhao, L. L. Gao, T. P. Ying, B. Gao, N. N. Li, W. G. Yang, D. Z. Zhang, H. Y. Gou, Y. L. Chen, H. Hosono, G. Li, and Y. P. Qi, Pressure-induced topological and structural phase transitions in an antiferromagnetic topological insulator, *Chin. Phys. Lett.* 37(6), 066401 (2020)
12. J. H. Li, Y. Li, S. Q. Du, Z. Wang, B. L. Gu, S. C. Zhang, K. He, W. H. Duan, and Y. Xu, Intrinsic magnetic topological insulators in van der Waals layered $MnBi_2Te_4$-family materials, *Sci. Adv.* 5(6), eaaw5685 (2019)
13. Y. J. Deng, Y. J. Yu, M. Z. Shi, Z. X. Guo, Z. H. Xu, J. Wang, X. H. Chen, and Y. Zhang, Quantum anomalous Hall effect in intrinsic magnetic topological insulator $MnBi_2Te_4$, *Science* 367(6480), 895 (2020)
14. J. Ge, Y. Z. Liu, J. H. Li, H. Li, T. C. Luo, Y. Wu, Y. Xu, and J. Wang, High-Chern-number and high-temperature quantum Hall effect without Landau levels, *Natl. Sci. Rev.* 7, 1280 (2020)
15. Z. Li, J. Li, K. He, X. Wan, W. Duan, and Y. Xu, Tunable interlayer magnetism and band topology in van der Waals heterostructures of $MnBi_2Te_4$-family materials, *Phys. Rev. B* 102(8), 081107 (2020) (R)
16. Y. Lai, L. Ke, J. Yan, R. D. McDonald, and R. J. McQueeney, Defect-driven ferrimagnetism and hidden magnetization in $MnBi_2Te_4$, *Phys. Rev. B* 103(18), 184429 (2021)
17. W. Zhu, C. Song, L. Liao, Z. Zhou, H. Bai, Y. Zhou, and F. Pan, Quantum anomalous Hall insulator state in ferromagnetically ordered $MnBi_2Te_4/VBi_2Te_4$ heterostructures, *Phys. Rev. B* 102(8), 085111 (2020)
18. M. M. Otrokov, I. I. Klimovskikh, H. Bentmann, A. Zeugner, Z. S. Aliev, S. Gass, A. U. B. Wolter, A. V. Koroleva, D. Estyunin, A. M. Shikin, M. Blanco-Rey, M. Hoffmann, I. P. Rusinov, A. Yu. Vyazovskaya, S. V. Eremeev, Y. M. Koroteev, V. M. Kuznetsov, F. Freyse, J. Sánchez-Barriga, I. R. Amiraslanov, M. B. Babanly, N. T. Mamedov, N. A. Abdullayev, V. N. Zverev, A. Alfonsov, V. Kataev, and B. Büchner, E. F. Schwier, S. Kumar, A. Kimura, L. Petaccia, G. Di Santo, R. C. Vidal, S. Schatz, K. Kißner, M. Ünzelmann, C. H. Min, S. Moser, T. R. F. Peixoto, F. Reinert, A. Ernst, P. M. Echenique, A. Isaeva, and E. V. Chulkov, Prediction and observation of an antiferromagnetic topological insulator, *Nature* 576(7787), 416 (2019)
19. S. Changdar, S. Ghosh, K. Vijay, I. Kar, S. Routh, P. K. Maheshwari, S. Ghorai, S. Banik, and S. Thirupathaiah, Nonmagnetic Sn doping effect on the electronic and magnetic properties of antiferromagnetic topological insulator $MnBi_2Te_4$, *Physica B* 657, 414799 (2023)
20. A. Zeugner, F. Nietschke, A. U. B. Wolter, S. Gaß, R. C. Vidal, T. R. F. Peixoto, D. Pohl, C. Damm, A. Lubk, R. Hentrich, S. K. Moser, C. Fornari, C. H. Min, S. Schatz, K. Kißner, M. Ünzelmann, M. Kaiser, F. Scaravaggi, B. Rellinghaus, K. Nielsch, C. Hess, B. Büchner,

F. Reinert, H. Bentmann, O. Oeckler, T. Doert, M. Ruck, and A. Isaeva, Chemical aspects of the candidate antiferromagnetic topological insulator $MnBi_2Te_4$, *Chem. Mater.* 31, 2795 (2019)

21. T. Qian, Y. T. Yao, C. Hu, E. Feng, H. Cao, I. I. Mazin, T. R. Chang, and N. Ni, Magnetic dilution effect and topological phase transitions in $(Mn_{1-x}Pb_x)Bi_2Te_4$, *Phys. Rev. B* 106, 045121 (2022)
22. A. V. Tarasov, T. P. Makarova, D. A. Estyunin, A. V. Eryzhenkov, I. I. Klimovskikh, V. A. Golyashov, K. A. Kokh, O. E. Tereshchenko, and A. M. Shikin, Topological phase transitions driven by Sn doping in $(Mn_{1-x}Sn_x)Bi_2Te_4$, *Symmetry (Basel)* 15(2), 469 (2023)
23. M. M. Otrokov, T. V. Menshchikova, M. G. Vergniory, I. P. Rusinov, A. Y. Vyazovskaya, Y. M. Koroteev, G. Bihlmayer, A. Ernst, P. M. Echenique, A. Arnau, Highly-ordered wide bandgap materials for quantized anomalous Hall and magnetoelectric effects, *2D Mater.* 4(2), 025082 (2017)
24. Y. J. Hao, P. F. Liu, Y. Feng, X. M. Ma, E. F. Schwier, M. Arita, S. Kumar, C. W. Hu, R. E. Lu, M. Zeng, Y. Wang, Z. Y. Hao, H. Y. Sun, K. Zhang, J. W. Mei, N. Ni, L. S. Wu, K. Shimada, C. Y. Chen, Q. H. Liu, and C. Liu, Gapless surface Dirac cone in antiferromagnetic topological insulator $MnBi_2Te_4$, *Phys. Rev. X* 9(4), 041038 (2019)
25. T. F. Cao, D. F. Shao, K. Huang, G. T. Gurung, and E. Y. Tsymbal, Switchable anomalous Hall effects in polar-stacked 2D antiferromagnet $MnBi_2Te_4$, *Nano Lett.* 23(9), 3781 (2023)
26. D. S. Lee, T. H. Kim, C. H. Park, C. Y. Chung, Y. S. Lim, W. S. Seo, and H. H. Park, Crystal structure, properties and nanostructuring of a new layered chalcogenide semiconductor, Bi_2MnTe_4, *CrystEngComm* 15(27), 5532 (2013)
27. S. H. Lee, Y. Zhu, Y. Wang, L. Miao, T. Pillsbury, H. Yi, S. Kempinger, J. Hu, C. A. Heikes, P. Quarterman, W. Ratcliff, J. A. Borchers, H. Zhang, X. Ke, D. Graf, N. Alem, C. Z. Chang, N. Samarth, and Z. Mao, Spin scattering and noncollinear spin structure-induced intrinsic anomalous Hall effect in antiferromagnetic topological insulator $MnBi_2Te_4$, *Phys. Rev. Res.* 1(1), 012011 (2019)
28. R. Peng, T. Zhang, Z. He, Q. Wu, Y. Dai, B. Huang, and Y. Ma, Intrinsic layer-polarized anomalous Hall effect in bilayer $MnBi_2Te_4$, *Phys. Rev. B* 107(8), 085411 (2023)
29. J. Zhu, M. Naveed, B. Chen, Y. Du, J. Guo, H. Xie, and F. Fei, Magnetic and electrical transport study of the antiferromagnetic topological insulator Sn-doped $MnBi_2Te_4$, *Phys. Rev. B* 103(14), 144407 (2021)
30. J. Q. Yan, Z. L. Huang, W. Wu, A. F. May, W. D. Wu, and A. F. May, Vapor transport growth of $MnBi_2Te_4$ and related compounds, *J. Alloys Compd.* 906, 164327 (2022)
31. J. M. D. Coey, Magnetism, magnetic materials, *Cambridge University Press*, 9780511845000 (2010)
32. J. Q. Yan, S. Okamoto, M. A. McGuire, A. F. May, R. J. McQueeney, and B. C. Sales, Evolution of structural, magnetic, and transport properties in $MnBi_{2-x}Sb_xTe_4$, *Phys. Rev. B* 100(10), 104409 (2019)
33. P. A. Lee and T. V. Ramakrishnan, Disordered electronic systems, *Rev. Mod. Phys.* 57(2), 287 (1985)
34. B. L. Altshuler, D. Khmel'nitzkii, A. I. Larkin, and P. A. Lee, Magnetoresistance and Hall effect in a disordered two-dimensional electron gas, *Phys. Rev. B* 22(11), 5142 (1980)
35. J. Kondo, Resistance minimum in dilute magnetic alloys, *Prog. Theor. Phys.* 32(1), 37 (1964)
36. F. Y. Wu, Q. Y. Wu, C. Zhang, Y. Luo, X. Liu, Y. F. Xu, D. H. Lu, M. Hashimoto, H. Liu, Y. Z. Zhao, J. J. Song, Y. H. Yuan, H. Y. Liu, J. He, Y. X. Duan, Y. F. Guo, and J. Q. Meng, Itinerant to relocalized transition of electrons in the Kondo insulator $CeRu_4Sn_6$, *Front. Phys.* 18(5), 53304 (2023)
37. H. Z. Lu and S. Q. Shen, Weak antilocalization and localization in disordered and interacting Weyl semimetals, *Phys. Rev. B* 92(3), 035203 (2015)
38. H. Liu, J. Fan, H. Zheng, J. Wang, C. Ma, H. Wang, L. Zhang, C. Wang, Y. Zhu, and H. Yang, Magnetic properties and critical behavior of quasi-2D layered Cr_4Te_5 thin film, *Front. Phys.* 18(1), 13302 (2023)
39. M. Xu, L. Guo, L. Chen, Y. Zhang, S. S. Li, W. Zhao, X. Wang, S. Dong, and R. K. Zheng, Emerging weak antilocalization effect in $Ta_{0.7}Nb_{0.3}Sb_2$ semimetal single crystals, *Front. Phys.* 18(1), 13304 (2023)
40. H. T. Liu, Y. Z. Xue, J. A. Shi, R. A. Guzman, P. P. Zhang, Z. Zhou, Y. G. He, C. Bian, L. G. Wu, R. S. Ma, J. C. Chen, J. H. Yan, H. T. Yang, C. M. Shen, W. Zhou, L. H. Bao, and H. J. Gao, Observation of the Kondo effect in multilayer single-crystalline VTe_2 nanoplates, *Nano Lett.* 19(12), 8572 (2019)
41. D. R. Hamann, New solution for exchange scattering in dilute alloys, *Phys. Rev.* 158(3), 570 (1967)
42. T. P. Estyunina, A. M. Shikin, D. A. Estyunin, A. V. Eryzhenkov, I. I. Klimovskikh, K. A. Bokai, V. A. Golyashov, K. A. Kokh, O. E. Tereshchenko, S. Kumar, K. Shimada, and A. V. Tarasov, Evolution of $Mn_{1-x}Ge_xBi_2Te_4$ electronic structure under variation of Ge content, *Nanomaterials (Basel)* 13(14), 2151 (2023)